

## **Inhibitor potency varies widely among tumor-relevant human isocitrate dehydrogenase 1 mutants**

Diego Avellaneda Matteo, Grace A. Wells, Lucas A. Luna, Adam J. Grunseth, Olga Zagnitko, David A. Scott, An Hoang, Amit Luthra, Manal A. Swairjo, Jamie M. Schiffer, and Christal D. Sohl

### **Supplementary Material**

Supplementary Methods

Supplementary Table 1

Supplementary Table 2

Supplementary Table 3

Supplementary Table 4

Supplementary Table 5

Supplementary Figures S1-S11

Supplementary Material References

## SUPPLEMENTARY DATA

### Small angle X-ray scattering (SAXS) analysis

SAXS was used to assess the quality and features of each of the IDH1 protein constructs. SAXS data were collected on the Bio-SAXS beamline BL4–2 at the Stanford Synchrotron Research Laboratory using a Rayonix MX225-HE CCD detector (Rayonix, Evanston, IL, USA) with a sample-to-detector distance of 1.7 m and a beam energy of 11 keV ( $\lambda = 1.127 \text{ \AA}$ ). The momentum transfer (scattering vector)  $q$  was defined as  $q = 4\pi \sin(\theta)/\lambda$ , where  $2\theta$  is the scattering angle. The  $q$  scale was calibrated by silver behenate powder diffraction. All data were collected to a maximum  $q$  of  $0.4 \text{ \AA}^{-1}$ . Scattering data were collected from the buffer alone and subtracted from the total protein solution scattering. For all samples, a 100  $\mu\text{L}$  sample containing 42  $\mu\text{M}$  of protein was prepared in buffer containing 20 mM Tris–HCl (pH 7.5 at ambient temperature), 100 mM NaCl, 1 mM DTT and specific ligands. For WT IDH1 and R132Q IDH1, 500  $\mu\text{M}$  ICT, 100  $\mu\text{M}$  NADP<sup>+</sup>, and 10mM CaCl<sub>2</sub> were added. For R132Q and R132H IDH1, 500  $\mu\text{M}$   $\alpha\text{KG}$ , 100  $\mu\text{M}$  NADPH, and 10mM CaCl<sub>2</sub> were added. CaCl<sub>2</sub> was used to prevent catalytic turnover, but allow the required conformational change to occur [1]. SAXS experiments were also performed on apo enzymes under the same buffer conditions (20 mM Tris–HCl (pH 7.5) and 100 mM NaCl). Radii of gyration ( $R_g$ ), extrapolated from the Guinier region of the Guinier plot, were computed using PRIMUS [2, 3].  $P(r)$  functions were calculated using the program GNOM [4]. Theoretical scattering curves were computed from different structural models and compared to experimental scattering curves using the program FoXS [5, 6]. The structural parameters derived from the SAXS data are summarized in Supplementary Table S1, with experimental scattering data and Kratky plots shown in Supplementary Figure S2, show excellent consistency among WT and mutant forms of the protein in terms of protein size and folding. The apo form of the structure is larger, as the protein appears to clamp down over its substrates upon binding. The Porod-Debye exponent provides a new and reliable means for identifying flexibility in SAXS experiments [7]. Therefore, to check any dynamic transition during catalysis, we determined the Porod-Debye exponent ( $P$ ), deduced from the SAXS data. The consist values of Porod-Debye exponent,  $P$ , in all states further corroborate the absence of flexibility.

**Table S1. Parameters for SAXS analysis**

|   | [Protein]<br>( $\mu\text{M}$ ) <sup>a</sup> | $R_g$ (Å) from<br>Guinier plot <sup>b,c</sup> | $I(0)$ <sup>c</sup> | Porod-Debye<br>exponent<br>(P) <sup>d</sup> | MM (Da) <sup>e</sup> |
|---|---|---|---------------------|---|----------------------|
| WT IDH1 <sup>apo</sup>                            | 42  | $32.9 \pm 0.1$                                | 124.22              | 2.2   | 102.72               |
| WT IDH1 <sup>ICT+NADPH</sup>                      | 42  | $32.1 \pm 0.1$                                | 135.44              | 2.1   | 95.27                |
| R132Q IDH1 <sup>apo</sup>                         | 42  | $33.3 \pm 0.2$                                | 129.79              | 2.2   | 105.60               |
| R132Q IDH1 <sup>ICT+NADPH</sup>                   | 42  | $32.3 \pm 0.2$                                | 132.92              | 2.2   | 94.90                |
| R132Q IDH1 <sup><math>\alpha</math>KG+NADPH</sup> | 42  | $32.02 \pm 0.08$                              | 136.57              | 2.2   | 96.84                |
| R132H IDH1 <sup>apo</sup>                         | 42  | $34 \pm 1$                                    | 126.82              | 2.2   | 105.38               |
| R132H IDH1 <sup><math>\alpha</math>KG+NADPH</sup> | 42  | $32 \pm 2$                                    | 121.66              | 2.1   | 96.13                |

<sup>a</sup>Molarity is based on the dimeric conformation.

<sup>b</sup>The radius of gyration ( $R_g$ ) is the root mean squared distance (RMSD) from the center of mass to each electron.

<sup>c</sup>Determined by Guinier approximation in PRIMUS [2].

<sup>d</sup>The Porod-Debye exponents were calculated using the program Scatter (<https://bl1231.als.lbl.gov/scatter/>).

<sup>e</sup>Molecular masses (MM) are calculated by SAXSMoW (<http://saxs.ifsc.usp.br/>). Molecular mass from the protein sequence was determined to be 96,000 Da.

**Table S2. Characterization of IDH1 crystal structures without inhibitors bound**

| PDB               | Mutant/<br>Isoform | Substrates<br>Bound  | Surface<br>area<br>buried by<br>all<br>ligands | Open<br>versus<br>Closed<br>(Angles –<br>Figure 4C) | $\alpha$ 4/11-<br>$\alpha$ 10 (Å) | R132-D275<br>Distances<br>(mon1/mon2) | SiteMap<br>buried<br>volume<br>(Site 1,<br>Site 2)<br>Å <sup>3</sup> | $\alpha$ 10<br>density | Resolution<br>(Å) | Missing Side<br>Chains  |
|-------------------|--------------------|--|--|---|-----------------------------------|---------------------------------------|--|------------------------|-------------------|---|
| 1T0L<br>[8]       | WT                 | NADP <sup>+</sup> ,<br>isocitrate, Ca <sup>2+</sup>  | 873.94   | 66.3°/66.0°   | 20.12,<br>19.79                   | 4.57, 4.14                            | 75.89,<br>83.05  | no                     | 2.41              | none  |
| 1T09<br>[8]       | WT                 | NADP <sup>+</sup>  | 908.27   | 70.1°, 65.3°  | 23.56,<br>20.8                    | 5.53, 13.19                           |  | unraveled              | 2.7               | none  |
| 5YFM <sup>a</sup> | WT                 | NADP <sup>+</sup> , Mg <sup>2+</sup>   | 874.02   | 76.4°, 76.2°  | 25.29,<br>25.28                   | 5.92, 5.88                            | 58.82,<br>73.23  | no                     | 2.4               | K81, K233   |
| 4L03<br>[9]       | WT                 | NADP <sup>+</sup> , $\alpha$ KG,<br>Ca <sup>2+</sup> , ethylene<br>glycol bound in<br>to inhibitor<br>pocket | 618.35   | 65.2°, 65.2°  | 20.02,<br>23.1                    | 6.05, 6.09                            | 65.90,<br>87.04  | no                     | 2.1               | K3, K81,<br>E174, K350,<br>K3, E36, K65,<br>K81, K151,<br>E174, K350,<br>Q411, K413 |
| 4L04<br>[9]       | WT                 | NADP <sup>+</sup> , $\alpha$ KG,<br>Ca <sup>2+</sup>   | 972.05   | 65.7°, 66.9°  | 19.36,<br>19.00                   | 6.07, 6.8                             | 76.10,<br>95.65  | no                     | 2.87              | E36, E80,<br>K81, E174,<br>K187, K233,<br>E262, K350,<br>K406, K413,<br>S415        |
| 3MAR<br>[1]       | R132H              | NADP <sup>+</sup>  | 860  |   |                                   | not resolved                          |  | yes                    | 3.41              | none  |
| 3MAP<br>[1]       | R132H              | NADP <sup>+</sup> ,<br>isocitrate  | 955.64   |   |                                   | not resolved                          |  | yes                    | 2.8               | R140, V281,<br>Q283, Y285,<br>Y272  |
| 3MAS<br>[1]       | R132H              | NADP <sup>+</sup> ,<br>isocitrate  | 956.25   |   |                                   | not resolved                          |  | yes                    | 3.2               | none  |
| 4KZO<br>[9]       | R132H              | NADP <sup>+</sup> , $\alpha$ KG,<br>Ca <sup>2+</sup>   | 735.63   | 65.0°, 65.1°  | 17.68,<br>17.95                   | 7.10, 7.15                            | 57.07,<br>80.4   | no                     | 2.2               | K3, K81,<br>E174, E36,<br>K151, K350,<br>Q411, K413                                 |
| 4UMY<br>[10]      | R132H              | NADP <sup>+</sup>  | 787.911  |   |                                   | not resolved                          |  | yes                    | 2.07              | none  |
| 3INM<br>[11]      | R132H              | NADPH, $\alpha$ KG,<br>Ca <sup>2+</sup>  | 762.31   | 67.9°, 68.4°  | 18.38,<br>18.29                   | 7.05, 6.95                            | 55.27,<br>69.03  | no                     | 2.1               | none  |

<sup>a</sup>To be published

**Table S3. Characterization of IDH1 crystal structures with inhibitors bound**

| PDB              | Substrates Bound                  | Surface area buried by all ligands | Angle        | $\alpha$ 4/11- $\alpha$ 10 (Å) | R132-D275 Distances (mon1/2) (Å) | SiteMap buried volume (Site 1 + Site 2) Å <sup>3</sup> | $\alpha$ 10 density          | Resolution (Å) | Missing Side Chains   | Inhibitor type       | Inhibitor to monomer ratio |
|------------------|-----------------------------------|------------------------------------|--------------|--------------------------------|----------------------------------|--|------------------------------|----------------|---|----------------------|----------------------------|
| 5SUN [12]        | Inhibitor NADPH                   | 1466.04                            |              | -                              | not resolved                     |  | Absent                       | 2.477          | none  | neither              | 1 to 1                     |
| 5TQH [13]        | Inhibitor NADPH                   | 1506.41                            |              | -                              | not resolved                     |  | Absent                       | 2.2            | none  | neither              | 1 to 1                     |
| 6B0Z [14]        | Inhibitor NADPH                   | 1768.67                            | 106.2°       | 27.3                           | 9.64                             | N/A <sup>a</sup>                                       | N-terminal missing (chain A) | 2.34           | none  | neither              | 3 to 2                     |
| 5LGE [15]        | Inhibitor NADPH                   | 1160.88                            | 108°, 54.3°  | 21.5, 21.83                    | 7.95, 8.93                       | 412.84   | Present                      | 2.7            | none (but there are overlapping atoms)  | indole               | 1 to 2                     |
| 5L58 [16]        | Inhibitor NADPH                   | 1708.17                            |              | -                              | not resolved                     |  | Missing                      | 3.04           | Q138, T142, D160, N171, E173, E174, I215, L216, K217, K218  | adamantane           | 1 to 1                     |
| 5L57 [16]        | Inhibitor NADPH                   | 1694.84                            | 79.0°, 87.2° | 34.5, 30.61                    | 8.19, 7.16                       | N/A <sup>a</sup>                                       | Present                      | 2.695          | R100, Y135, Y167, K212, Y219, Y272, V281, K413,   | adamantane           | 1 to 1                     |
| 4UMX [10]        | Inhibitor NADP <sup>+</sup>       | 1123.92                            | 59.7°, 66.0° | 19.81, 20.78                   | 7.98, 13.95                      | N/A <sup>a</sup>                                       | Chain B missing              | 1.88           | none  | imidazole            | 1 to 2                     |
| 5DE1 [17]        | Inhibitor NADP <sup>+</sup>       | 1558.4                             |              |                                | not resolved                     |  | Missing                      | 2.25           | K3, K81, R140, K212, K243, D279, K350, K413, E62, E80, K93, Y135, R140, K164, E174, K217, K233, K270, | imidazole and indole | 1 to 1                     |
| 5SVF [12]        | Inhibitor NADPH and citrate anion | 1350.91                            |              |                                | not resolved                     |  | Missing                      | 2.34           | none  | neither              | 1 to 1                     |
| 5I96 (IDH2) [18] | Inhibitor NADPH, Ca <sup>2+</sup> | 967.9                              | 79.8°, 80.7° | 26.4, 24.8                     | 9.25, 10.36                      | 241.13   | Missing                      | 1.55           | none  | indole               | 1 to 2                     |

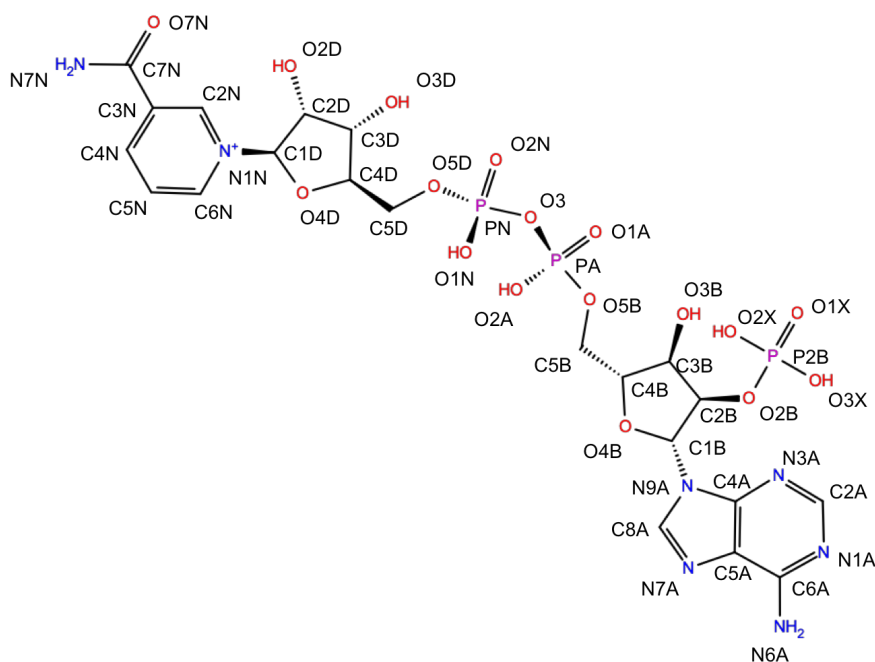
<sup>a</sup> Sites 1 and 2 (Supplementary Figure S4) merge together, join with the NADP<sup>+</sup> binding site of one chain, and become solvent accessible.

**Table S4. Distance between  $\alpha 1$  and  $\alpha 8$  – opening of IDH1 monomers**

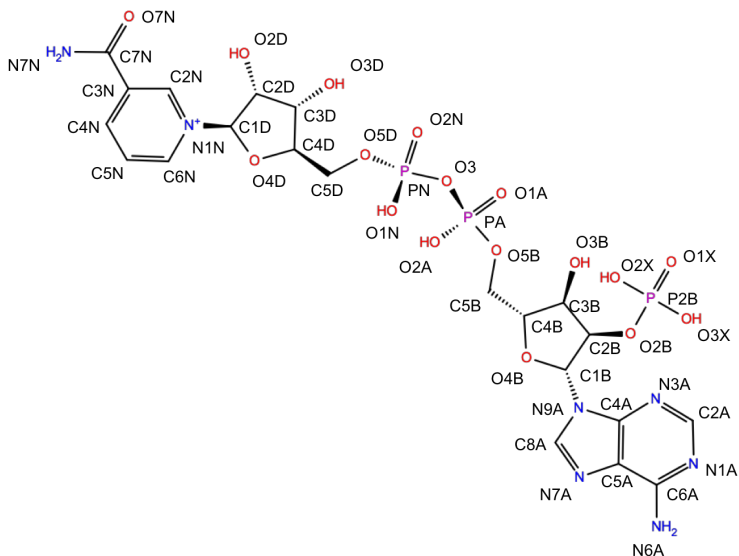
|                 | R132 (WT), Å        |                  | R132H, Å            |                  | R132Q, Å            |                  | R132L, Å            |                  |
|-----------------|---------------------|------------------|---------------------|------------------|---------------------|------------------|---------------------|------------------|
|                 | No Ca <sup>2+</sup> | Ca <sup>2+</sup> | No Ca <sup>2+</sup> | Ca <sup>2+</sup> | No Ca <sup>2+</sup> | Ca <sup>2+</sup> | No Ca <sup>2+</sup> | Ca <sup>2+</sup> |
| <b>MonomerA</b> | 31 ± 3              | 30 ± 3           | 27.9 ± 0.9          | 30 ± 2           | 28 ± 1              | 31 ± 4           | 28 ± 1              | 28.8 ± 0.9       |
| <b>MonomerB</b> | 34 ± 4              | 35 ± 4           | 27.8 ± 0.9          | 30 ± 2           | 28 ± 1              | 29.2 ± 0.9       | 27.4 ± 0.8          | 30 ± 3           |

**Table S5. NADP<sup>+</sup> RMSF from all-atom simulations**

Color scheme: ribose of adenine (green), adenine (gray), phosphates (yellow), ribose of nicotinamide (orange), nicotinamide (blue).



|             | R132H, Å |       | R132Q, Å |       | R132L, Å |       | R132, Å |       |
|-------------|----------|-------|----------|-------|----------|-------|---------|-------|
|             | Mon1     | Mon2  | Mon1     | Mon2  | Mon1     | Mon2  | Mon1    | Mon2  |
| <b>C4B</b>  | 4.232    | 4.949 | 3.601    | 4.334 | 3.611    | 4.924 | 4.496   | 4.187 |
| <b>H4B</b>  | 4.201    | 4.779 | 3.657    | 4.388 | 3.732    | 4.972 | 4.693   | 4.322 |
| <b>O4B</b>  | 4.101    | 5.036 | 3.526    | 4.462 | 3.52     | 5.045 | 4.445   | 4.241 |
| <b>C1B</b>  | 4.258    | 5.415 | 3.633    | 4.695 | 3.795    | 5.405 | 4.815   | 4.537 |
| <b>H1B</b>  | 4.361    | 5.586 | 3.796    | 4.897 | 3.875    | 5.534 | 5.137   | 4.755 |
| <b>C5A</b>  | 4.804    | 5.977 | 3.913    | 4.705 | 4.184    | 5.766 | 4.668   | 4.788 |
| <b>N7A</b>  | 4.753    | 5.866 | 3.673    | 4.625 | 3.975    | 5.442 | 4.778   | 4.8   |
| <b>C8A</b>  | 4.477    | 5.638 | 3.517    | 4.598 | 3.758    | 5.276 | 4.732   | 4.694 |
| <b>H8A</b>  | 4.489    | 5.543 | 3.393    | 4.589 | 3.597    | 5.078 | 4.883   | 4.879 |
| <b>N9A</b>  | 4.37     | 5.604 | 3.657    | 4.652 | 3.853    | 5.464 | 4.685   | 4.555 |
| <b>N1A</b>  | 5.371    | 6.388 | 4.563    | 4.989 | 4.748    | 6.507 | 4.876   | 5.351 |
| <b>C2A</b>  | 5.246    | 6.289 | 4.588    | 5.008 | 4.694    | 6.515 | 5.04    | 5.262 |
| <b>H2A</b>  | 5.602    | 6.49  | 4.938    | 5.191 | 4.966    | 6.885 | 5.401   | 5.65  |
| <b>N3A</b>  | 4.884    | 6.022 | 4.305    | 4.896 | 4.417    | 6.18  | 4.971   | 4.911 |
| <b>C4A</b>  | 4.628    | 5.853 | 3.947    | 4.736 | 4.141    | 5.804 | 4.707   | 4.68  |
| <b>C6A</b>  | 5.177    | 6.243 | 4.232    | 4.831 | 4.519    | 6.125 | 4.728   | 5.089 |
| <b>N6A</b>  | 5.508    | 6.416 | 4.306    | 4.863 | 4.692    | 6.171 | 4.844   | 5.318 |
| <b>H61A</b> | 5.558    | 6.416 | 4.34     | 4.799 | 4.753    | 6.016 | 4.939   | 5.516 |
| <b>H62A</b> | 5.885    | 6.319 | 4.49     | 5.037 | 4.875    | 6.4   | 5.091   | 5.463 |

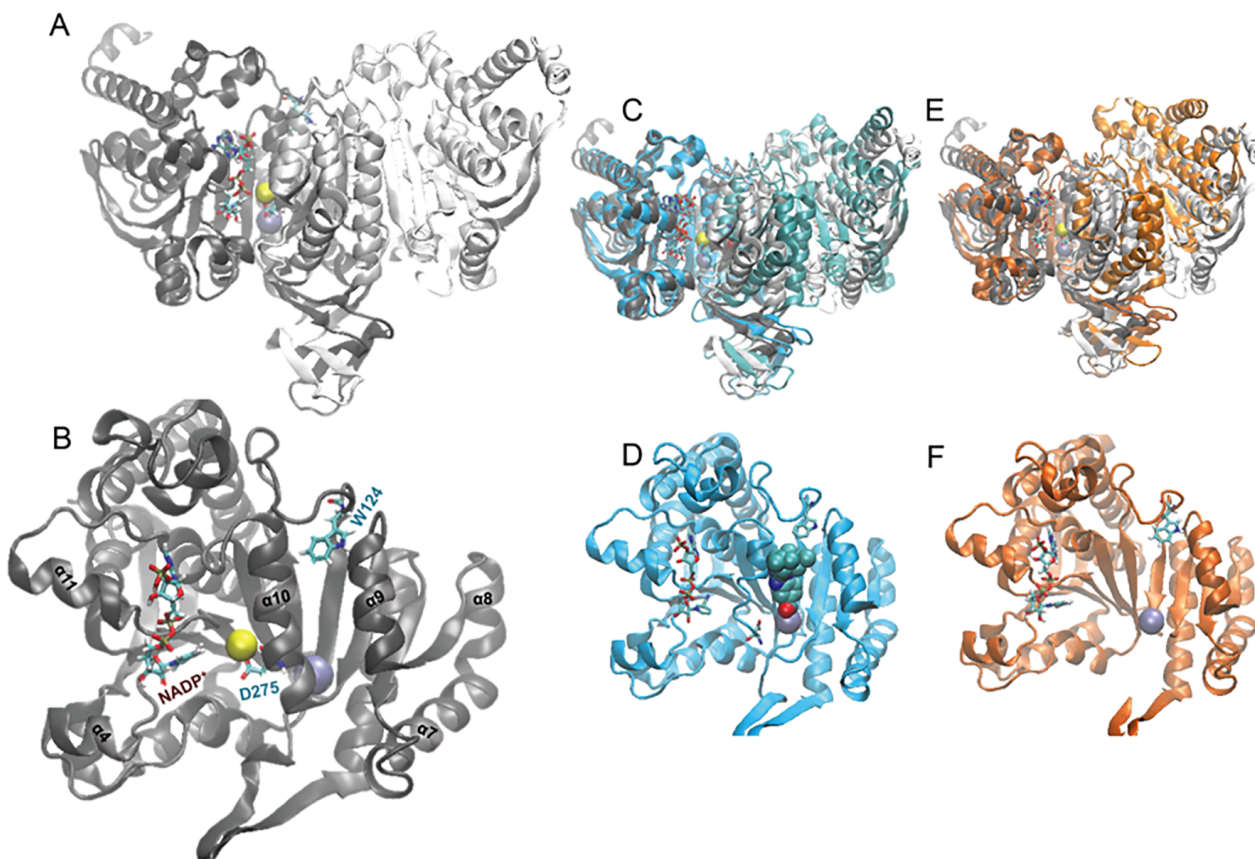


|      | R132H, Å |       | R132Q, Å |       | R132L, Å |       | R132, Å |       |
|------|----------|-------|----------|-------|----------|-------|---------|-------|
|      | Mon1     | Mon2  | Mon1     | Mon2  | Mon1     | Mon2  | Mon1    | Mon2  |
| C2B  | 4.434    | 6.651 | 3.641    | 4.827 | 4.048    | 5.64  | 5.16    | 4.747 |
| H2B  | 4.497    | 5.519 | 3.655    | 4.835 | 4.225    | 5.812 | 5.132   | 4.709 |
| O2B  | 4.59     | 5.686 | 3.785    | 5.473 | 4.23     | 6.225 | 5.888   | 5.314 |
| P2B  | 4.991    | 5.699 | 3.865    | 5.884 | 4.568    | 6.73  | 6.54    | 5.682 |
| O1X  | 5.331    | 6.213 | 4.288    | 5.98  | 4.964    | 7.18  | 7.137   | 6.006 |
| O2X  | 5.183    | 6.503 | 4.094    | 6.332 | 4.714    | 6.979 | 6.825   | 5.705 |
| O3X  | 5.388    | 6.476 | 4.082    | 6.321 | 4.845    | 6.908 | 6.735   | 6.355 |
| HO2A | 5.703    | 6.61  | 4.332    | 6.581 | 4.894    | 6.973 | 7.025   | 6.755 |
| C3B  | 4.642    | 6.829 | 3.793    | 4.475 | 4.006    | 5.199 | 4.95    | 4.581 |
| H3B  | 4.948    | 5.447 | 3.998    | 4.404 | 4.061    | 5.077 | 4.978   | 4.567 |
| O3B  | 5.036    | 5.825 | 4.058    | 4.638 | 4.422    | 5.42  | 5.446   | 4.95  |
| HO3A | 5.294    | 5.612 | 4.353    | 4.849 | 4.587    | 5.714 | 5.866   | 5.312 |
| C5B  | 4.244    | 5.806 | 3.533    | 4.126 | 3.34     | 4.647 | 4.189   | 3.788 |
| H51A | 4.391    | 4.797 | 3.58     | 4.098 | 3.462    | 4.525 | 4.404   | 3.896 |
| H52A | 4.148    | 4.721 | 3.534    | 4.138 | 3.2      | 4.648 | 4.137   | 3.768 |
| PA   | 4.522    | 4.681 | 3.65     | 4.029 | 3.14     | 4.692 | 4.134   | 3.457 |
| O1A  | 4.956    | 5.342 | 4.25     | 4.637 | 3.009    | 5.25  | 4.621   | 3.505 |
| O2A  | 4.668    | 5.795 | 3.872    | 4.016 | 3.233    | 4.784 | 4.119   | 3.485 |
| O5B  | 4.426    | 5.699 | 3.625    | 4.104 | 3.377    | 4.718 | 4.19    | 3.645 |
| O3   | 4.435    | 5.115 | 3.543    | 4.054 | 3.534    | 4.582 | 4.246   | 3.718 |
| PN   | 4.487    | 5.041 | 3.598    | 4.003 | 3.536    | 4.501 | 4.393   | 3.741 |
| O1N  | 4.38     | 5.155 | 3.459    | 3.695 | 3.355    | 4.354 | 4.336   | 3.721 |
| O2N  | 4.616    | 5.37  | 3.968    | 4.329 | 3.765    | 4.836 | 4.76    | 4.228 |
| O5D  | 4.792    | 5.194 | 3.774    | 4.187 | 3.931    | 4.479 | 4.52    | 3.586 |
| C5D  | 5.266    | 5.161 | 4.003    | 4.595 | 4.314    | 4.772 | 4.939   | 3.825 |
| H51N | 5.369    | 5.196 | 4.126    | 4.687 | 4.395    | 4.932 | 4.99    | 3.882 |

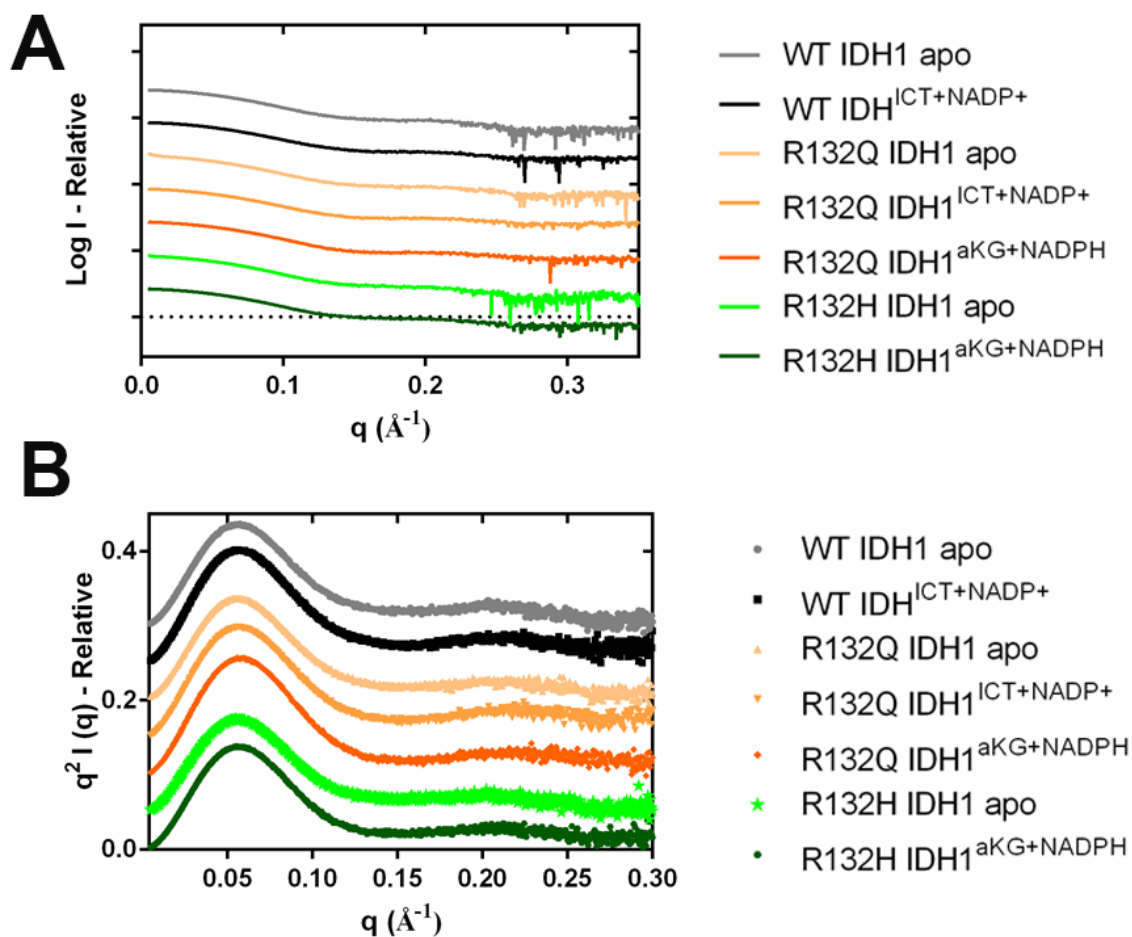
(cont. on next page)



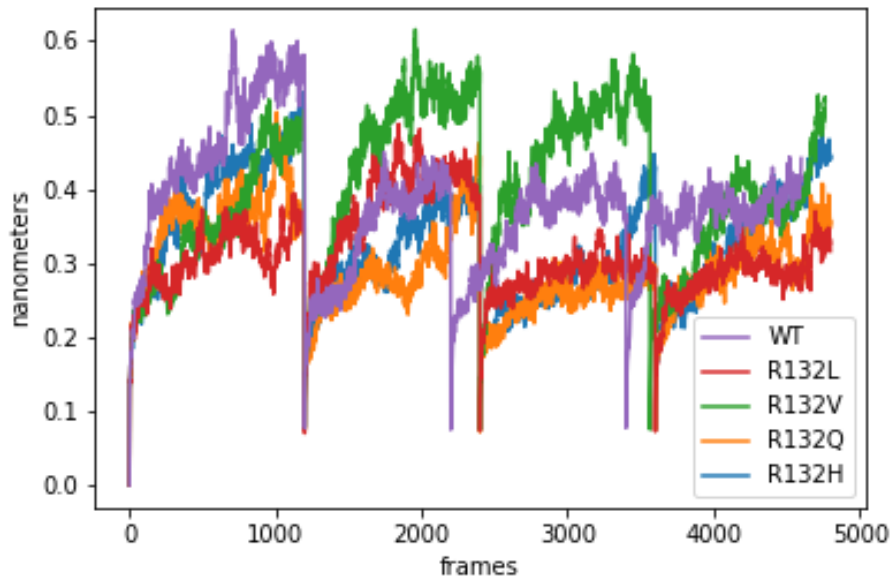
|                | R132H, Å |         | R132Q, Å |        | R132L, Å |        | R132, Å |       |
|----------------|----------|---------|----------|--------|----------|--------|---------|-------|
|                | Mon1     | Mon2    | Mon1     | Mon2   | Mon 1    | Mon 2  | Mon1    | Mon2  |
| H52N           | 5.427    | 5.29    | 4.202    | 4.739  | 4.468    | 4.989  | 5.298   | 4.215 |
| C2D            | 5.4      | 5.208   | 3.748    | 4.632  | 4.408    | 4.639  | 5.007   | 3.771 |
| H2D            | 5.015    | 5.04    | 3.623    | 4.342  | 4.101    | 4.471  | 4.674   | 3.823 |
| O2D            | 5.718    | 4.912   | 3.863    | 4.814  | 4.623    | 4.837  | 5.417   | 3.972 |
| HO2N           | 5.627    | 5.074   | 3.945    | 4.869  | 4.71     | 5.179  | 5.447   | 4.155 |
| C3D            | 5.736    | 5.129   | 3.99     | 4.902  | 4.662    | 4.811  | 5.427   | 4.076 |
| H3D            | 5.642    | 5.13    | 4.048    | 4.812  | 4.572    | 4.831  | 5.497   | 4.308 |
| O3D            | 6.344    | 5.031   | 4.227    | 5.34   | 5.101    | 5.043  | 6.074   | 4.554 |
| HO3N           | 6.383    | 5.314   | 4.115    | 5.254  | 5.114    | 4.899  | 6.372   | 4.943 |
| C1D            | 5.406    | 5.191   | 3.736    | 4.669  | 4.474    | 4.642  | 4.837   | 3.514 |
| H1D            | 5.785    | 5.174   | 3.898    | 4.96   | 4.799    | 4.875  | 5.273   | 3.629 |
| C4D            | 5.615    | 5.28    | 4.016    | 4.853  | 4.598    | 4.823  | 5.178   | 3.867 |
| C4D            | 5.615    | 5.215   | 4.258    | 5.18   | 4.902    | 5.123  | 5.577   | 4.237 |
| H4D            | 6.018    | 5.321   | 3.871    | 4.735  | 4.534    | 4.698  | 4.907   | 4.237 |
| O4D            | 5.477    | 5.261   | 3.871    | 4.735  | 4.534    | 4.698  | 4.907   | 3.587 |
| N1N            | 5.04     | 5.147   | 3.545    | 4.362  | 4.193    | 4.457  | 4.328   | 3.466 |
| C6N            | 4.692    | 5.02    | 3.46     | 4.026  | 3.85     | 4.177  | 3.846   | 3.431 |
| HN6            | 4.68     | 4.952   | 3.564    | 3.981  | 3.768    | 4.109  | 3.864   | 3.409 |
| C5N            | 4.513    | 5.04    | 3.35     | 3.814  | 3.686    | 4.082  | 3.597   | 3.641 |
| H5N            | 4.416    | 4.984   | 3.367    | 3.602  | 3.466    | 3.914  | 3.47    | 3.702 |
| C4N            | 4.628    | 5.2     | 3.327    | 3.952  | 3.885    | 4.313  | 3.793   | 3.993 |
| H41N           | 4.569    | 5.26    | 3.303    | 3.843  | 3.842    | 4.316  | 3.761   | 4.395 |
| C3N            | 4.983    | 5.342   | 3.457    | 4.304  | 4.212    | 4.649  | 4.287   | 3.993 |
| C2N            | 5.202    | 5.312   | 3.553    | 4.495  | 4.356    | 4.692  | 4.554   | 3.672 |
| H2N            | 5.624    | 5.473   | 3.73     | 4.816  | 4.673    | 5.002  | 5.1     | 3.755 |
| C7N            | 5.281    | 5.596   | 3.634    | 4.538  | 4.49     | 5.045  | 4.744   | 4.56  |
| O7N            | 5.752    | 5.863   | 3.988    | 4.998  | 4.849    | 5.504  | 5.393   | 4.793 |
| N7N            | 5.186    | 5.61    | 3.642    | 4.351  | 4.438    | 5.06   | 4.663   | 5.077 |
| H71N           | 4.966    | 5.748   | 3.629    | 4.22   | 4.276    | 5.19   | 4.643   | 5.124 |
| H72N           | 5.479    | 5.754   | 3.834    | 4.545  | 4.659    | 5.319  | 5.03    | 5.478 |
| <b>Average</b> | 5.02481  | 5.53124 | 3.8577   | 4.6703 | 4.2014   | 5.2196 | 4.9407  | 4.444 |
| <b>STD</b>     | 0.55     | 0.52    | 0.34     | 0.58   | 0.53     | 0.77   | 0.75    | 0.76  |



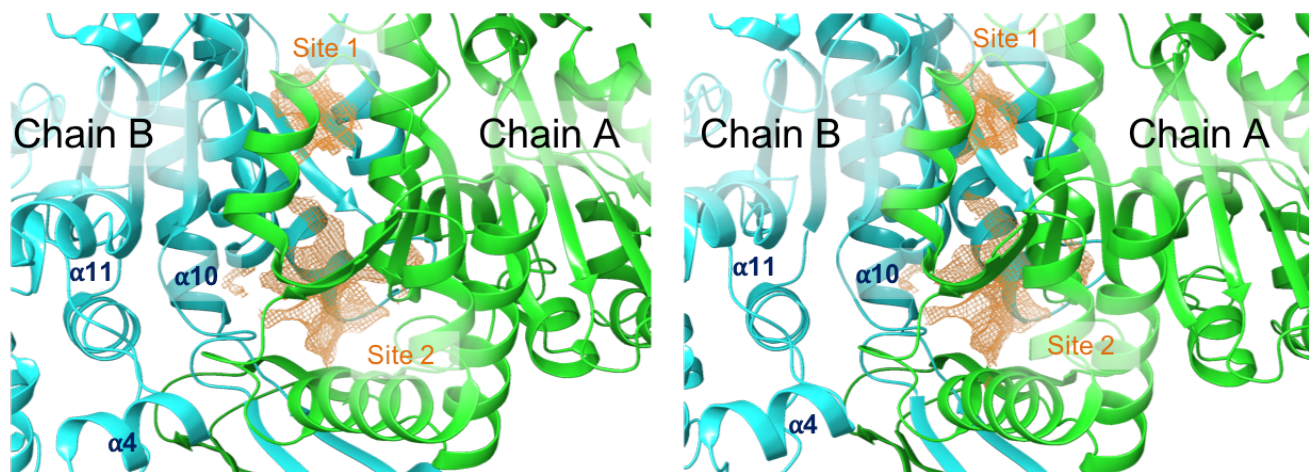
**Supplementary Figure S1. A comparison of previously solved structures of WT and mutant IDH1 bound to NADP<sup>+</sup> used in MD simulations.** The structure of IDH1 bound to NADP<sup>+</sup> used here for MD simulations (PDB 4KZO [9]) is shown for both dimers (A) and as monomeric secondary structure units (B). Structures were aligned to monomer A (left monomer in gray). In both panels, the C<sub>α</sub> carbon of residue 132 is shown as a sphere (ice blue), as is Ca<sup>2+</sup> (yellow). The residues W124, D275, and NADP<sup>+</sup> are shown as licorice with the carbon in cyan, the oxygen in red, the phosphorus is gold, nitrogen in blue, and hydrogen in white. The helices that are discussed in the text are labeled as indicated previously [8]. (C) The structure of IDH1 bound to NADP<sup>+</sup> versus the structure of IDH1 R132H bound to an analogue of BAY 1436032 (PDB 5LGE) is shown [15]. (D) The secondary structure units of IDH1 R132H bound to the inhibitor described in (C) is displayed in its monomeric form [15]. (E) The structure of IDH1 bound to NADP<sup>+</sup> versus the structure of IDH1 R132H bound to the inhibitor IDH146 (PDB 5SUN) is shown [12]. (F) The structure of the monomeric secondary structure units of IDH1 R132H bound to NADPH is displayed.



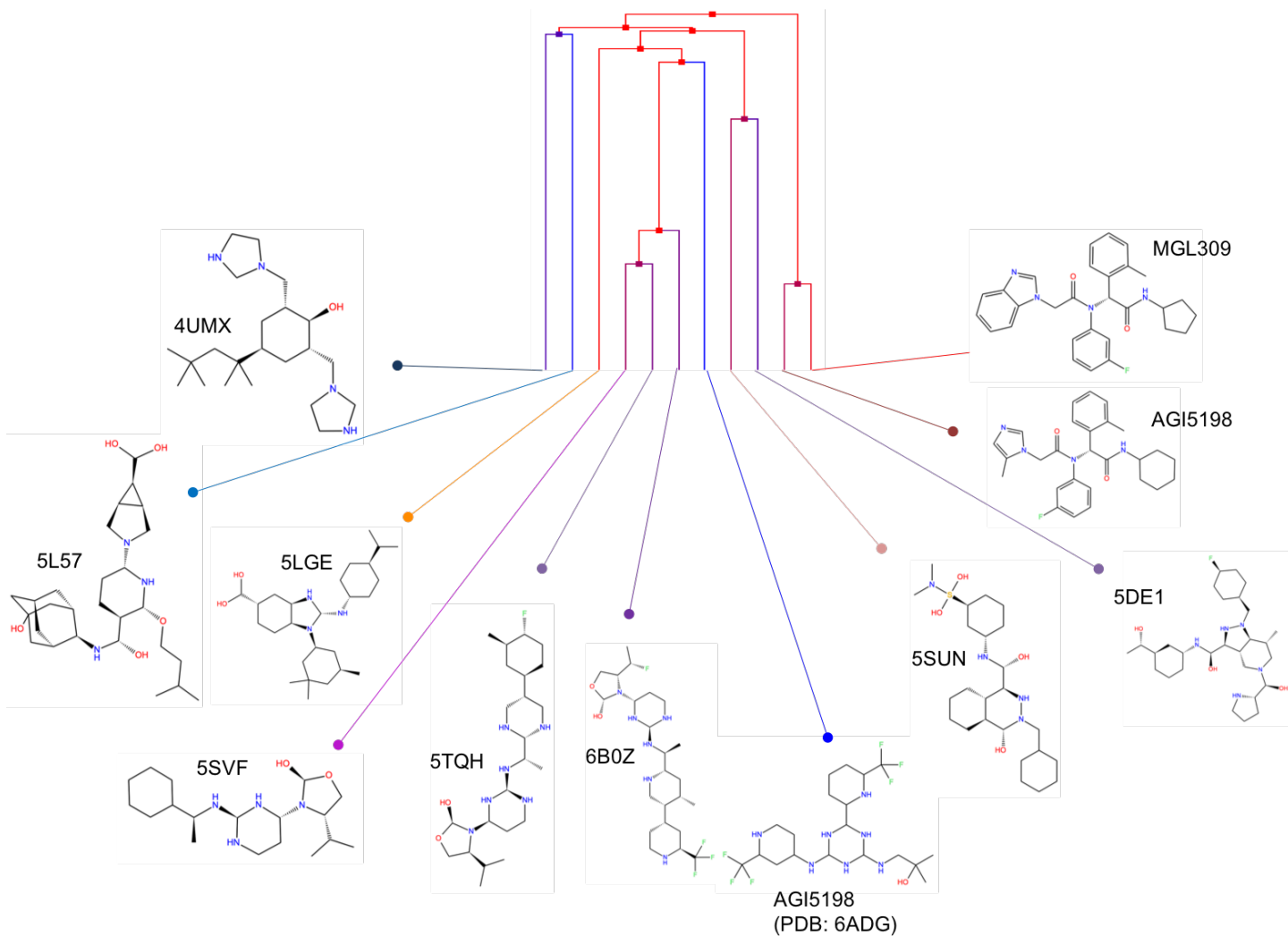
**Supplementary Figure S2. Small angle X-ray scattering (SAXS) data for apo and ligand-bound forms of WT and mutant IDH1.** (A) Experimental scattering curves for WT IDH1<sup>apo</sup> (grey), WT IDH1<sup>ICT and NADP+</sup> (black), R132Q IDH1<sup>apo</sup> (light orange), R132Q IDH1<sup>ICT and NADP+</sup> (orange), R132Q IDH1 <sup>$\alpha$ KG and NADPH</sup> (dark orange), R132H IDH1<sup>apo</sup> (light green), and R132H IDH1 <sup>$\alpha$ KG and NADPH</sup> (dark green). (B) Kratky plots derived from SAXS data. The color scheme of graphs is identical to those used in panel (A).



**Supplementary Figure S3. RMSD analysis of IDH1 simulations.** The RMSD over time for all five systems studied (WT IDH1 in purple, R132L IDH1 in red, R132V IDH1 in green, R132Q IDH1 in orange, and R132H IDH1 in blue) are shown across frames for all four replicates. WT, R132L, R132Q and R132H IDH1 follow similar trajectories, reaching equilibrium by the end of the frame.

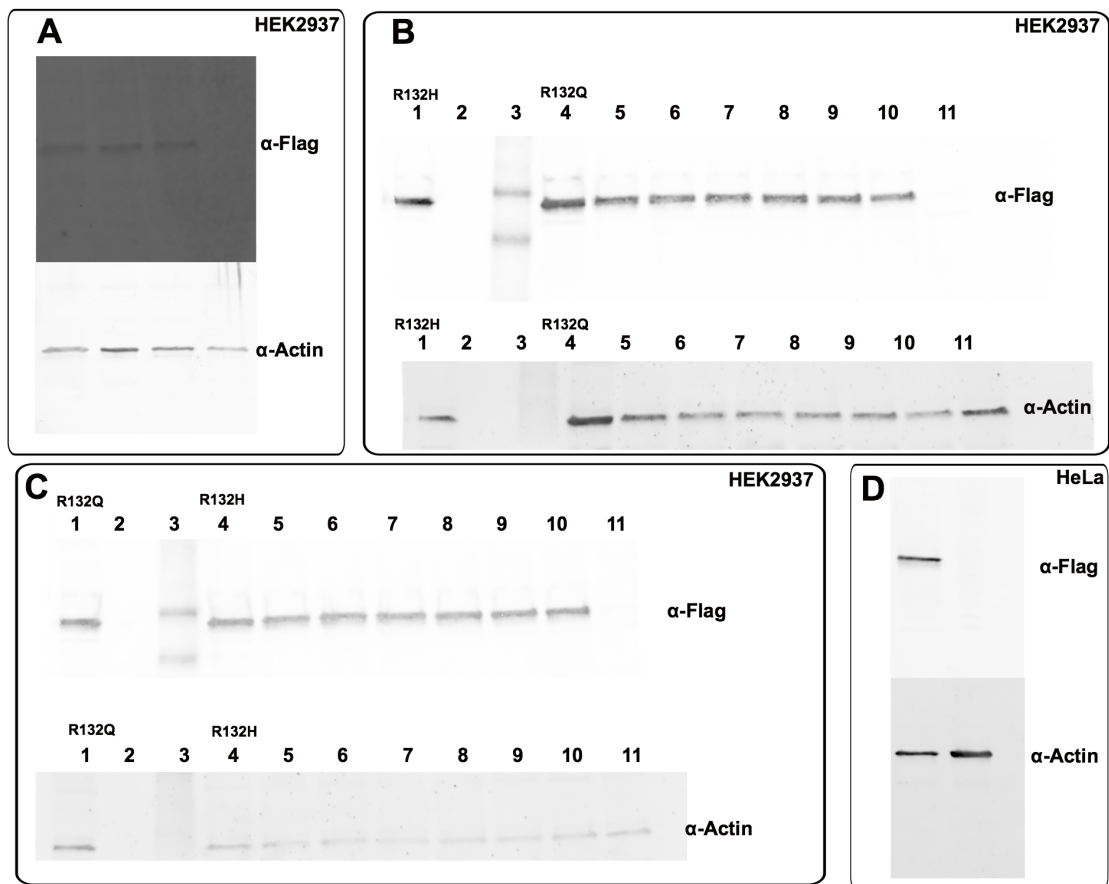


**Supplementary Figure S4. Buried cavity shape of crystal structures.** Two small, solvent-inaccessible pockets located between the  $\alpha 9$  and  $\alpha 10$  helices are highlighted as Site 1 and Site 2 in the previously solved crystal structures of PDB 4KZO [9]. Images are taken from two slightly different angles.



**Supplementary Figure S5. Clustering of IDH1/2 Inhibitors based on linear fingerprints of each structure.**

Hierarchical clustering results performed within Canvas on the linear fingerprints of inhibitors known to bind to IDH1 from X-ray crystallography or of inhibitors used in this study. The inhibitors described in this work were grouped into their own hierarchical cluster separate from the crystallized inhibitors.



**Supplementary Figure S6. Levels of transient overexpression of R132H and R132Q IDH1 in HEK293T**

**cells vary within 2.6-fold.** (A) Transient transfection of WT IDH1 (lane 1), R132Q IDH1 (lane 2), R132H IDH1

(lane 3) all containing a Flag-tag, and a non-transfected HEK293T control. Whole cell lysates of HEK293T cells

transiently transfected with R132Q or R132H IDH1 were loaded as follows: (B) 1. R132H; 2. Empty; 3. Ladder;

4. R132Q; 5. R132Q + 20 nM AGI-5198; 6. R132Q + 40 nM AGI-5198; 7. R132Q + 90 nM AGI-5198; 8. R132Q

+ 180 nM AGI-5198; 9. R132Q + 500 nM AGI-9198; 10. R132Q + 3,000 nM AGI-5198; 11. Non-transfected

control. (C) 1. R132Q; 2. Empty; 3. Ladder; 4. R132H; 5. R132H + 20 nM AGI-5198; 6. R132H + 40 nM AGI-

5198; 7. R132H + 90 nM AGI-5198; 8. R132H + 180 nM AGI-5198; 9. R132H + 500 nM AGI-9198; 10. R132H +

3,000 nM AGI-5198; 11. Non-transfected control. Upon normalizing to actin, panel (B) indicates R132H

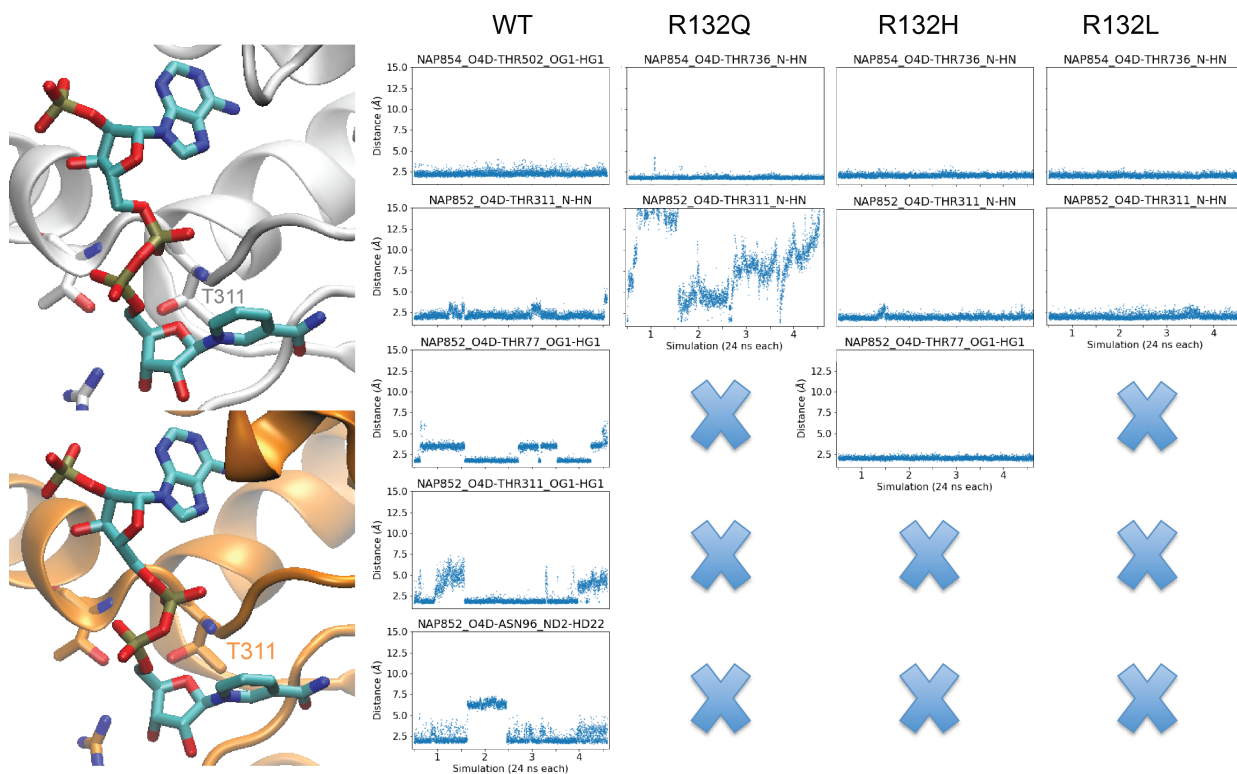
expression is 3.0-fold higher than R132Q IDH1, and panel (C) indicates that R132H IDH1 is 2.3-fold higher than

R132Q IDH1. Thus, we took the average of these two values (3.0 and 2.3) to calculate that R132H IDH1 has

2.6-fold higher expression relative to R132Q IDH1 expression. (D) Transient transfection of HeLa cells with

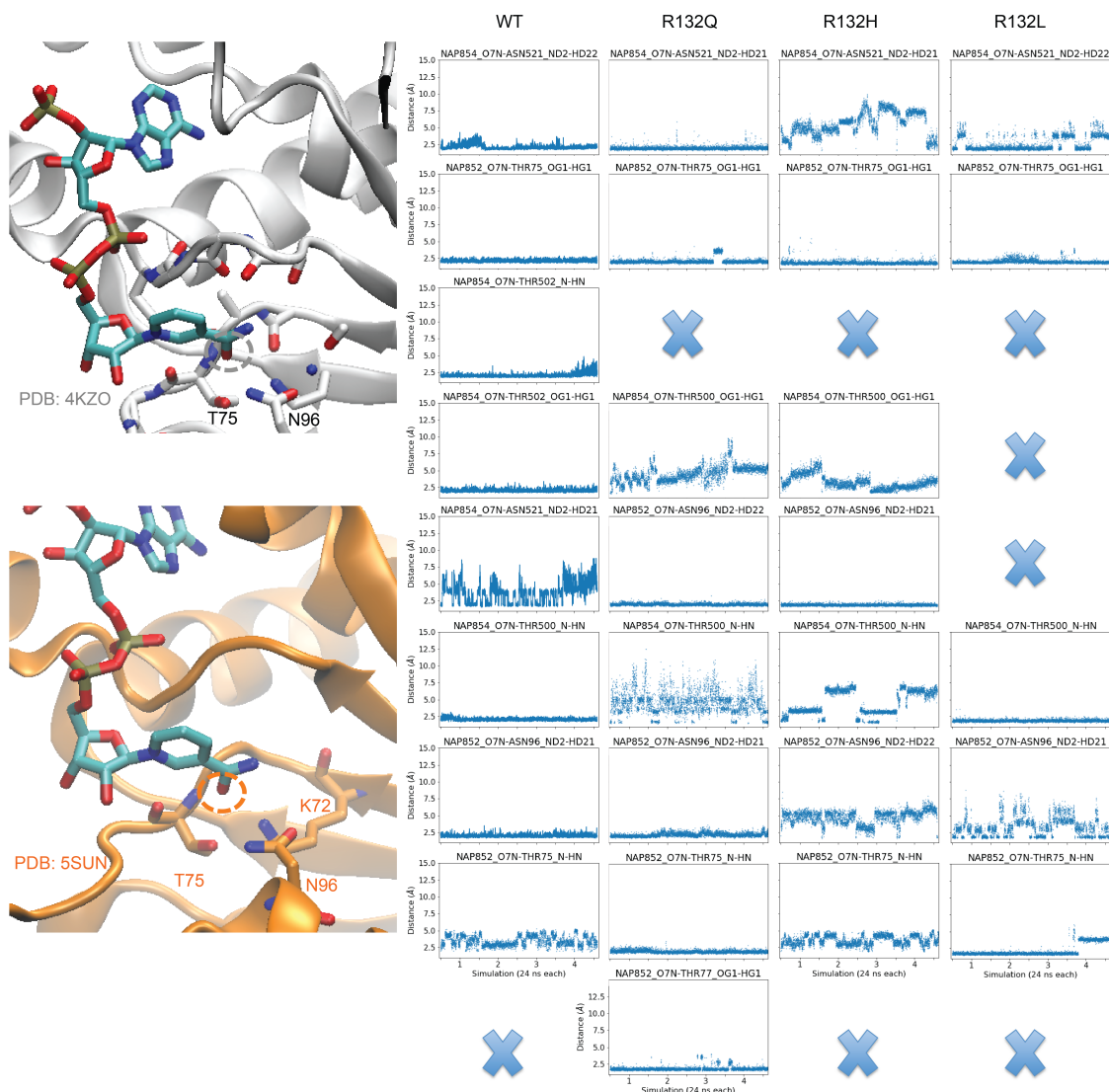
R132Q IDH1 is also shown. Lane one shows the R132Q IDH1 transfection (Flag-tagged), and lane 2 shows a

non-transfected HeLa control.

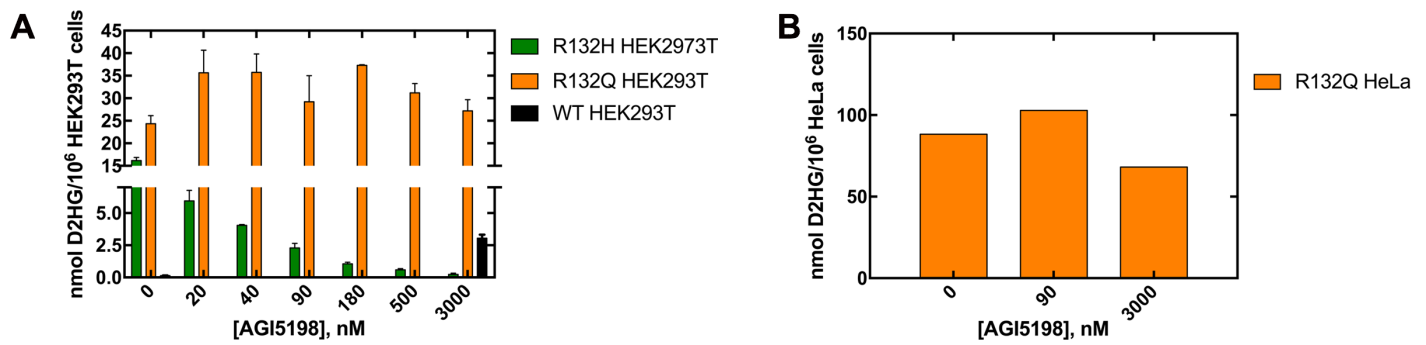


**Supplementary Figure S7. Hydrogen bonding interactions between mutants and WT IDH1 and the NADP<sup>+</sup> ribose oxygen vary over MD simulations.** The hydrogen bond distance between the ester oxygen of the nicotinamide riboside and neighboring threonine residues as compared to crystal structures of NADP<sup>+</sup>-bound (white, top) and NADPH-bound (orange, below). This region of the molecule shows minimal differences in hydrogen bonding patterns when IDH1 is bound to NADP<sup>+</sup> versus NADPH. Stable hydrogen bond interactions are shown as a constant clustering around 2.5 Å, while stochastic fluctuations show periods where hydrogen bonding is favorable or unfavorable. Hydrogen bonding that is impossible due to inappropriate bond lengths or angles are denoted as an “x” for the hydrogen bond donor/acceptor pair queried. WT IDH1 makes the most hydrogen bond interactions with the ester oxygen of the nicotinamide riboside portion of NADP<sup>+</sup>, while the mutants show varying degree of hydrogen bond formation in this region. This region is likely less useful for comparing features of NADP<sup>+</sup> versus NADPH binding.

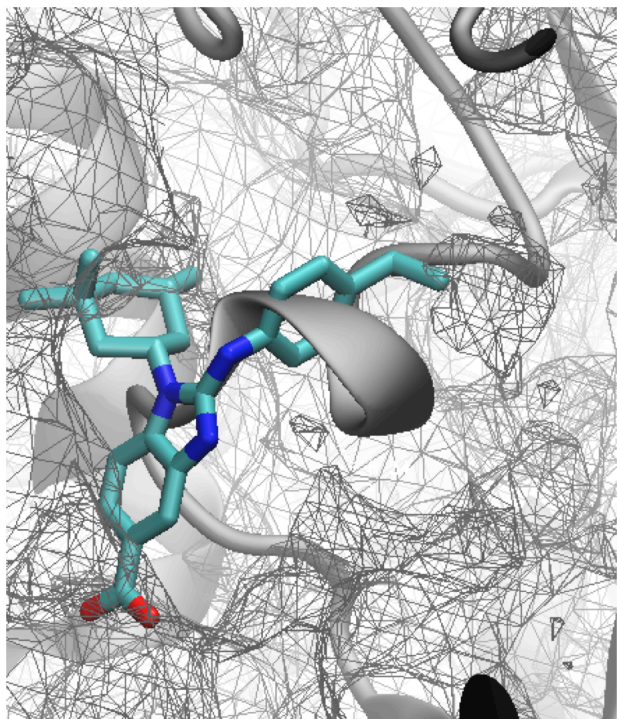




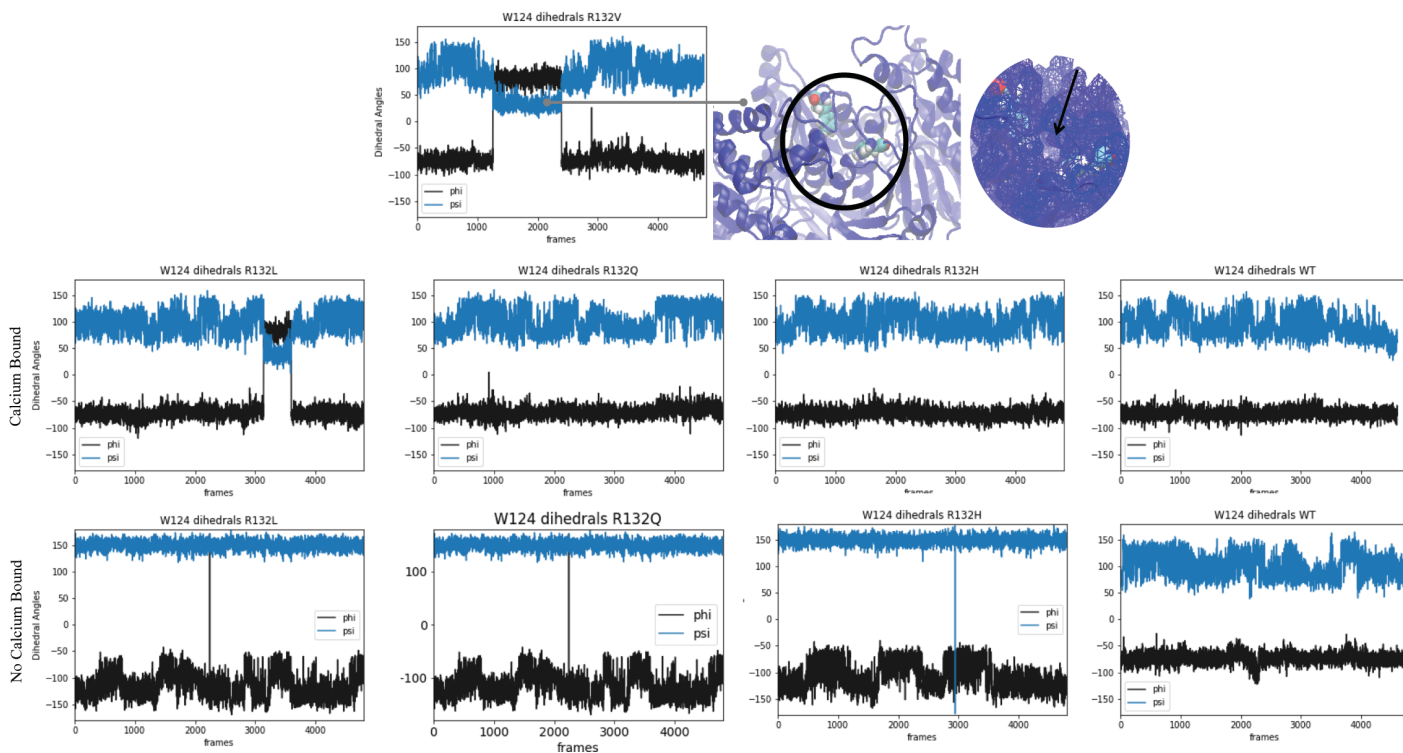
**Supplementary Figure S8. Hydrogen bonding interactions between mutants and WT IDH1 and the NADP<sup>+</sup> amide oxygen vary over MD simulations.** The hydrogen bond distance between the amide oxygen of the nicotinamide and neighboring threonine and arginine residues as compared to crystal structures of NADP<sup>+</sup>-bound (white, top) and NADPH-bound (orange, below). This region of the molecule shows differences in hydrogen bonding patterns when IDH1 is bound to NADP<sup>+</sup> versus NADPH, indicating that this region is a good differentiator between NADP<sup>+</sup> versus NADPH binding. Stable hydrogen bond interactions are shown as a constant clustering around 2.5 Å, while stochastic fluctuations show periods where hydrogen bonding is favorable or unfavorable. Hydrogen bonding that is impossible due to inappropriate bond lengths or angles are denoted as an “x” for the hydrogen bond donor/acceptor pair queried. Here, R132L IDH1 has the fewest hydrogen bonds in the amide oxygen of the nicotinamide, while WT IDH1 has the most stable interactions. R132Q IDH1 has the largest number of stable hydrogen bonding interactions of all the mutants.



**Supplementary Figure S9. AGI-5198 does not effectively inhibit R132Q IDH1.** (A) Quantitation (in duplicate) of D2HG in lysates of HEK2937 cells transiently transfected with R132H, R132Q, or WT and treated with AGI-5198 is shown. These data were used to calculate  $IC_{50}$  values shown in Figure 5. (B) Quantitation (in singlicate) of D2HG in lysates of HeLa cells transiently transfected with R132Q IDH1 and treated with AGI-5198 is shown; only a subset of inhibitor concentrations were used.



**Supplementary Figure S10. Average buried cavity in the apo WT IDH1 simulation.** An analogue of the inhibitor BAY1436032 from PDB 5LGE [15] is overlaid with the apo WT IDH1 simulations, which start from PDB 1T09 [8].



**Supplementary Figure S11. Changes in the dihedral angle of residue W124 and the effects on an exposed buried cavity.** The dihedral angle changes for residue W124, which sits on top of the buried cavity at the dimer interface, are shown. In the R132L and R132V IDH1 simulations, one of four trajectories results in flipping of W124 and exposure of the buried cavity to a small pocket opening as depicted. The psi angle changes are shown in blue while the phi angle changes are shown in black.

## Supplementary Material References

- 1 Yang, B., Zhong, C., Peng, Y., Lai, Z. and Ding, J. (2010) Molecular mechanisms of "off-on switch" of activities of human IDH1 by tumor-associated mutation R132H. *Cell Res.* **20**, 1188-1200
- 2 Bauer, W. J., Luthra, A., Zhu, G., Radolf, J. D., Malkowski, M. G. and Caimano, M. J. (2015) Structural characterization and modeling of the *Borrelia burgdorferi* hybrid histidine kinase Hk1 periplasmic sensor: A system for sensing small molecules associated with tick feeding. *J Struct Biol.* **192**, 48-58
- 3 Konarev Petr, V., Volkov Vladimir, V., Sokolova Anna, V., Koch Michel, H. J. and Svergun Dmitri, I. PRIMUS: a Windows PC-based system for small-angle scattering data analysis. *J Appl Cryst.* **36**, 1277-1282
- 4 Svergun, D. I. (1992) Determination of the regularization parameter in indirect-transform methods using perceptual criteria. *J Appl Crystallogr.* **25**, 495-503
- 5 Schneidman-Duhovny, D., Hammel, M., Tainer, J. A. and Sali, A. (2013) Accurate SAXS profile computation and its assessment by contrast variation experiments. *Biophys J.* **105**, 962-974
- 6 Schneidman-Duhovny, D., Hammel, M., Tainer, J. A. and Sali, A. (2016) FoXS, FoXSDock and MultiFoXS: Single-state and multi-state structural modeling of proteins and their complexes based on SAXS profiles. *Nucleic Acids Res.* **44**, W424-429
- 7 Rambo, R. P. and Tainer, J. A. (2011) Characterizing flexible and intrinsically unstructured biological macromolecules by SAS using the Porod-Debye law. *Biopolymers.* **95**, 559-571
- 8 Xu, X., Zhao, J., Xu, Z., Peng, B., Huang, Q., Arnold, E. and Ding, J. (2004) Structures of human cytosolic NADP-dependent isocitrate dehydrogenase reveal a novel self-regulatory mechanism of activity. *J Biol Chem.* **279**, 33946-33957
- 9 Rendina, A. R., Pietrak, B., Smallwood, A., Zhao, H., Qi, H., Quinn, C., Adams, N. D., Concha, N., Duraiswami, C., Thrall, S. H., Sweitzer, S. and Schwartz, B. (2013) Mutant IDH1 enhances the production of 2-hydroxyglutarate due to its kinetic mechanism. *Biochemistry.* **52**, 4563-4577
- 10 Deng, G., Shen, J., Yin, M., McManus, J., Mathieu, M., Gee, P., He, T., Shi, C., Bedel, O., McLean, L. R., Le-Strat, F., Zhang, Y., Marquette, J. P., Gao, Q., Zhang, B., Rak, A., Hoffmann, D., Rooney, E., Vassort, A., Englaro, W., Li, Y., Patel, V., Adrian, F., Gross, S., Wiederschain, D., Cheng, H. and Licht, S. (2015) Selective inhibition of mutant isocitrate dehydrogenase 1 (IDH1) via disruption of a metal binding network by an allosteric small molecule. *J Biol Chem.* **290**, 762-774
- 11 Dang, L., White, D. W., Gross, S., Bennett, B. D., Bittinger, M. A., Driggers, E. M., Fantin, V. R., Jang, H. G., Jin, S., Keenan, M. C., Marks, K. M., Prins, R. M., Ward, P. S., Yen, K. E., Liau, L. M., Rabinowitz, J. D., Cantley, L. C., Thompson, C. B., Vander Heiden, M. G. and Su, S. M. (2009) Cancer-associated IDH1 mutations produce 2-hydroxyglutarate. *Nature.* **462**, 739-744
- 12 Xie, X., Baird, D., Bowen, K., Capka, V., Chen, J., Chenail, G., Cho, Y., Dooley, J., Farsidjani, A., Fortin, P., Kohls, D., Kulathila, R., Lin, F., McKay, D., Rodrigues, L., Sage, D., Toure, B. B., van der Plas, S., Wright, K., Xu, M., Yin, H., Levell, J. and Pagliarini, R. A. (2017) Allosteric mutant IDH1 inhibitors reveal mechanisms for IDH1 mutant and isoform selectivity. *Structure.* **25**, 506-513
- 13 Levell, J. R., Caferro, T., Chenail, G., Dix, I., Dooley, J., Firestone, B., Fortin, P. D., Giraldez, J., Gould, T., Growney, J. D., Jones, M. D., Kulathila, R., Lin, F., Liu, G., Mueller, A., van der Plas, S., Slocum, K., Smith, T., Terranova, R., Toure, B. B., Tyagi, V., Wagner, T., Xie, X., Xu, M., Yang, F. S., Zhou, L. X., Pagliarini, R. and Cho, Y. S. (2017) Optimization of 3-pyrimidin-4-yl-oxazolidin-2-ones as allosteric and mutant specific inhibitors of IDH1. *ACS Med Chem Lett.* **8**, 151-156
- 14 Cho, Y. S., Levell, J. R., Liu, G., Caferro, T., Sutton, J., Shafer, C. M., Costales, A., Manning, J. R., Zhao, Q., Sendzik, M., Shultz, M., Chenail, G., Dooley, J., Villalba, B., Farsidjani, A., Chen, J., Kulathila, R., Xie, X., Dodd, S., Gould, T., Liang, G., Heimbach, T., Slocum, K., Firestone, B., Pu, M., Pagliarini, R. and Growney, J. D. (2017) Discovery and evaluation of clinical candidate IDH305, a brain penetrant mutant IDH1 inhibitor. *ACS Med Chem Lett.* **8**, 1116-1121
- 15 Pusch, S., Krausert, S., Fischer, V., Balss, J., Ott, M., Schrimpf, D., Capper, D., Sahm, F., Eisel, J., Beck, A. C., Jugold, M., Eichwald, V., Kaulfuss, S., Panknin, O., Rehwinkel, H., Zimmermann, K., Hillig, R. C., Guenther, J., Toschi, L., Neuhaus, R., Haegbart, A., Hess-Stumpp, H., Bauser, M., Wick, W., Unterberg, A., Herold-Mende, C., Platten, M. and von Deimling, A. (2017) Pan-mutant IDH1 inhibitor BAY 1436032 for effective treatment of IDH1 mutant astrocytoma in vivo. *Acta Neuropathol.* **133**, 629-644
- 16 Jones, S., Ahmet, J., Ayton, K., Ball, M., Cockerill, M., Fairweather, E., Hamilton, N., Harper, P., Hitchin, J., Jordan, A., Levy, C., Lopez, R., McKenzie, E., Packer, M., Plant, D., Simpson, I., Simpson, P.,

Sinclair, I., Somervaille, T. C., Small, H., Spencer, G. J., Thomson, G., Tonge, M., Waddell, I., Walsh, J., Waszkowycz, B., Wigglesworth, M., Wiseman, D. H. and Ogilvie, D. (2016) Discovery and optimization of allosteric inhibitors of mutant isocitrate dehydrogenase 1 (R132H IDH1) displaying activity in human acute myeloid leukemia cells. *J Med Chem.* **59**, 11120-11137

17 Okoye-Okafor, U. C., Bartholdy, B., Cartier, J., Gao, E. N., Pietrak, B., Rendina, A. R., Rominger, C., Quinn, C., Smallwood, A., Wiggall, K. J., Reif, A. J., Schmidt, S. J., Qi, H., Zhao, H., Joberty, G., Faeltsh-Savitski, M., Bantscheff, M., Drewes, G., Duraiswami, C., Brady, P., Groy, A., Narayanagari, S. R., Antony-Debre, I., Mitchell, K., Wang, H. R., Kao, Y. R., Christopheit, M., Carvajal, L., Barreyro, L., Paietta, E., Makishima, H., Will, B., Concha, N., Adams, N. D., Schwartz, B., McCabe, M. T., Maciejewski, J., Verma, A. and Steidl, U. (2015) New IDH1 mutant inhibitors for treatment of acute myeloid leukemia. *Nat Chem Biol.* **11**, 878-886

18 Yen, K., Travins, J., Wang, F., David, M. D., Artin, E., Straley, K., Padyana, A., Gross, S., DeLaBarre, B., Tobin, E., Chen, Y., Nagaraja, R., Choe, S., Jin, L., Konteatis, Z., Cianchetta, G., Saunders, J. O., Salituro, F. G., Quivoron, C., Opolon, P., Bawa, O., Saada, V., Paci, A., Broutin, S., Bernard, O. A., de Botton, S., Marteyn, B. S., Pilichowska, M., Xu, Y., Fang, C., Jiang, F., Wei, W., Jin, S., Silverman, L., Liu, W., Yang, H., Dang, L., Dorsch, M., Penard-Lacronique, V., Biller, S. A. and Su, S. M. (2017) AG-221, a first-in-class therapy targeting acute myeloid leukemia harboring oncogenic IDH2 mutations. *Cancer Discov.* **7**, 478-493